

Recent progress of second harmonic generation based on thin film lithium niobate [Invited]

Yang Li (黎洋)¹, Zhijin Huang (黄志进)¹, Wentao Qiu (丘文涛)¹, Jiangli Dong (董江莉)², Heyuan Guan (关贺元)^{2*}, and Huihui Lu (卢惠辉)^{1**}

¹Guangdong Provincial Key Laboratory of Optical Fiber Sensing and Communications, Jinan University, Guangzhou 510632, China

²Key Laboratory of Optoelectronic Information and Sensing Technologies of Guangdong Higher Education Institutes, Jinan University, Guangzhou 510632, China

*Corresponding author: tguanheyuan@jnu.edu.cn

**Corresponding author: thuihui@jnu.edu.cn

Received February 25, 2021 | Accepted April 15, 2021 | Posted Online May 20, 2021

Recently, nonlinear photonics has attracted considerable interest. Among the nonlinear effects, second harmonic generation (SHG) remains a hot research topic. The recent development of thin film lithium niobate (TFLN) technology has superior performances to the conventional counterparts. Herein, this review article reveals the recent progress of SHG based on TFLN and its integrated photonics. We mainly discuss and compare the different techniques of TFLN-based structures to boost the nonlinear performances assisted by localizing light in nanostructures and structured waveguides. Moreover, our conclusions and perspectives indicate that more efficient methods need to be further explored for higher SHG conversion efficiency on the TFLN platform.

Keywords: thin film lithium niobate; second harmonic generation; waveguide; nanostructure.

DOI: [10.3788/COL202119.060012](https://doi.org/10.3788/COL202119.060012)

1. Introduction

Nonlinear effects of optics have been explored since Maxwell's time. However, much progress has been made in the field of nonlinear optics since the discovery of the laser, which made high-intensity optical fields easily feasible. The field started to grow with the first, to the best of our knowledge, experimental work of Franken *et al.* on optical second-harmonic generation (SHG) in 1961^[1]. In SHG, input pump light can be converted to a signal with twice the frequency. The efficient second-order nonlinear process is a promising platform for many kinds of applications such as light sources^[2,3], optical frequency conversion^[4], optical focusing^[5], supercontinuum generation^[6,7], and biological applications like local fluorescent excitation^[8]. For practical applications, it is of great significance to improve SHG conversion efficiency for the research on second-order nonlinear effects. Up to now, compact photonic micro- and nanostructures with enhanced optical nonlinearities at different wavelength ranges have been studied extensively. However, nonlinear optical performances still need to be improved^[9–11].

The lithium niobate (LiNbO₃, LN) crystal is one of the most promising materials to address a considerable number of optical applications^[12–14], well-known for its excellent nonlinear optic, piezoelectric, electro-optic (EO), photoelastic, and photorefractive properties in the present days. Indeed, LN is naturally

birefringent and has a broad transparency spectral window from the ultraviolet to the far infrared (350–5500 nm). Recently, due to the excellent optical properties of LN, the emerging LN technology has received great attention in the research of integrated and guided-wave optics. With the help of advanced micro-nano fabrication technologies, many high-performance LN integrated photonic devices have been realized^[15]. Levy *et al.* reported on the exfoliation of the first high-quality (Q) LN film from a piece of bulk LN crystal by ion slicing in 1998^[16]. Recently, thin film LN (TFLN) as a modern and emerging technology platform capable of tighter integration of nonlinear devices has been a topic of intense research and is uniquely well-suited for any functions requiring modulating light or shifting the frequency of light. TFLN can facilitate large-scale integration of photonic integrated circuits, as well as boost performance for optical devices compared to bulk LN crystals^[17–19]. Silicon is lack of high second-order susceptibilities ($\chi^{(2)}$) with more absorption losses. Moreover, the loss of TFLN-based devices is much lower than that of silicon-based optoelectronic devices^[20]. So far, the major applications of TFLN in nonlinear optics are well-developed second-order nonlinear processes.

As mentioned in Fig. 1, most nonlinear applications of TFLN are mainly divided into structured waveguides and nanostructures. Due to nonlinear effects that can be significantly enhanced

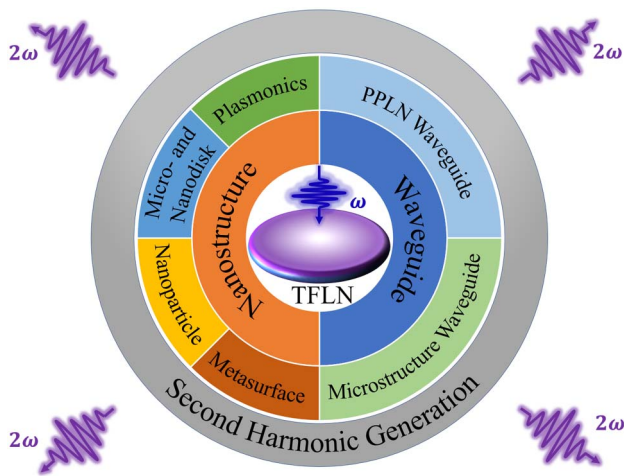


Fig. 1. Summary of different approaches of SHG based on TFLN technology.

inside nanophotonic waveguides with tight light confinement^[21–23], the most feasible approach to achieve near 100% nonlinear conversion efficiency is the waveguide. However, more recently, nanostructures made by TFLN supporting Fano resonances^[24] and Mie resonances^[25] are also widely used in phase-matching-free nonlinear optics fields such as compact SHG devices and integrated LN chips. In many cases, the nonlinear structures are optimized to realize and maximize their conversion efficiency.

In this paper, we briefly summarize the recent developments and progresses of SHG based on TFLN technology. The review will focus on different techniques for enhancing SHG conversion efficiency based on TFLN. Lastly, this article also summarizes the latest advances in the functionality of TFLN nonlinear photonic devices and gives a short outlook on their future applications in the fast-growing field of multifunctional integrated photonics.

2. Nonlinear Optical Structures Based on TFLN

2.1. Second harmonic generation in structured waveguides

SHG is the most straightforward nonlinear application of TFLN waveguides. In this section, we give a brief overview of the different waveguides in TFLN and discuss their developments. As mentioned before, TFLN can overcome the drawbacks associated with bulk LN devices. TFLN is oftentimes applied to the platform of LN-on-insulator (LNOI)^[26], like the silicon-on-insulator (SOI), although silicon or LN is sometimes used as a substrate. Generally speaking, the insulator layer is comprised of a lower refractive index material to avoid optical mode leakage from the thin film into the substrate, such as silicon dioxide (SiO₂). A high-Q LNOI substrate was recently commercialized by NANOLN Inc. in China, facilitating the area of photonics on the LNOI platform all over the world^[27]. Traditional LN waveguides are fabricated by titanium indiffusion or by proton exchange^[28], whereas waveguides in LNOI oftentimes are ridge

waveguides fabricated by reactive ion etching (RIE)^[29,30]. In this approach, the fabrication of TFLN-based optical elements requires advanced micro- and nanostructuring methods. SHG from waveguides has the advantages of combining the high optical power density inside the waveguides with the periodic modulation of nonlinear coefficients^[31]. For efficient second-order nonlinear optical interactions, phase-matching conditions need to be fulfilled because the wave propagation is linked to the wavelength-dependent refractive index^[32]. Various phase-matching techniques have been utilized in order to demonstrate thin film periodically poled LN (TF-PPLN) waveguides^[33]. To date, quasi-phase matching (QPM)^[34] as the most preferred approach to achieve phase matching can be achieved by inverting the spontaneous polarization of the optically ferroelectric crystals periodically along the waveguide to compensate the wave-vector mismatch Δk between the pump and SHG optical modes^[35,36]. Furthermore, the QPM technique allows a free choice of different polarizations of the interacting light waves^[37].

Recently, much effort has improved conversion efficiencies by combining the QPM of periodically poled LN (PPLN) with the strong field confinement of the waveguide. In TFLN, periodic poling is most commonly achieved by the application of a strong electric field along the z axis of the crystal through electrodes. PPLN is made by using a static electric field to invert the orientation of the ferroelectric domains in LN thin film^[38]. QPM SHG in bulk PPLN has been widely used among all the QPM wavelength converters with extremely high efficiencies in the visible and near infrared (NIR).

Here, we will first refer to QPM nonlinear devices, because QPM interactions in waveguides with quadratic nonlinearities enable highly efficient nonlinear frequency conversion. For example, monolithic nanophotonic PPLN waveguides used for light propagating along the y axis were successfully prepared by standard lithography on a high-Q periodically poled X -cut Mg-doped LN film [Fig. 2(a)]^[39]. As indicated in Fig. 2(b), the periodically poled LNOI (PPLNOI) waveguide fabricated by the electrical field poling technique with active monitoring of the poling fidelity on the nanophotonic chip was characterized by SHG at 1470 nm, with the normalized conversion efficiency as high as 3061% W⁻¹ cm⁻². Moreover, the reliability and repeatability of the LNOI platform can be improved by designing photonic structures with high tolerance to the fabrication errors^[40]. The nonlinear frequency converter is schematically illustrated in Fig. 2(c) for a PPLNOI ridge waveguide with simultaneous transverse EO coupling and efficient conversion for SHG, which holds promise in realizing electrically controllable on-chip nonlinear devices^[41]. A shallow-etched ridge waveguide has been fabricated in X -cut magnesium-oxide-doped TFLN, achieving the length-normalized conversion efficiency of 3757% W⁻¹ cm⁻² to indicate promising applications for robust and efficient waveguides^[42] [Fig. 2(d)].

More and more researches on various structures designed with periodically poled TFLN waveguides can further enhance SHG conversion efficiency. These structures can achieve

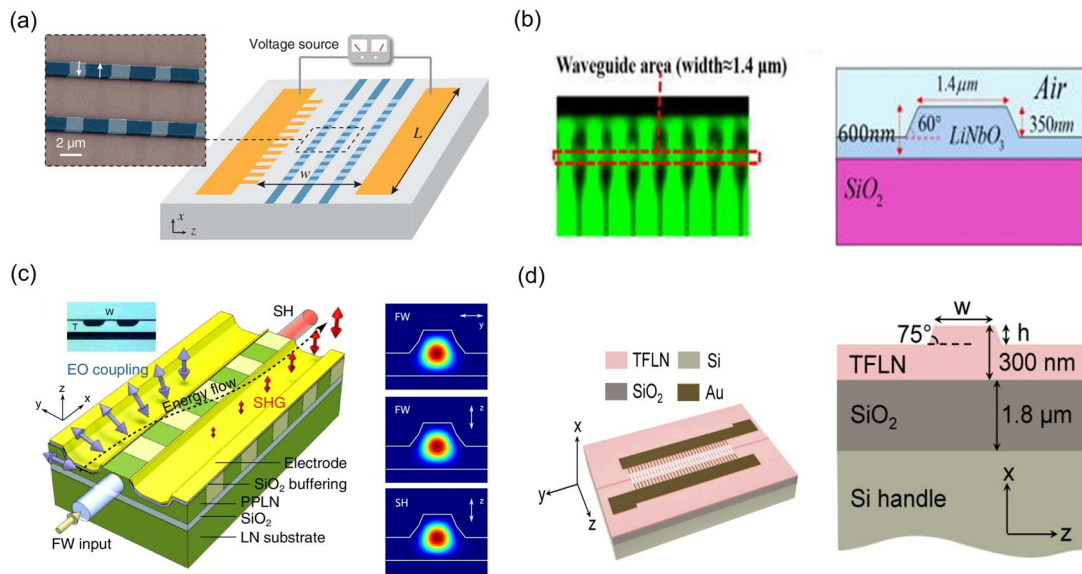


Fig. 2. (a) Schematic and false-color SEM image of a periodically poled nanophotonic waveguide^[39]; Copyright 2018, Optical Society of America. (b) SH confocal microscopy of the PPLN thin film fabricated by microelectrode poling and the cross section of the LNOI ridge waveguide^[40]; Copyright 2020, AIP Publishing. (c) Schematic of the cascading EO coupling and SHG process in the PPLN ridge waveguide^[41]; Copyright 2019, Optical Society of America. (d) Schematic illustration of the PPLN waveguide with poling electrodes^[42]; Copyright 2019, Optical Society of America.

efficient SHG via different phase-matching mechanisms, such as type I phase matching by tuning temperature^[43], modal phase matching by mode-shape modulation^[44], modal dispersion phase matching by modal dispersion engineering^[36], or grating-assisted QPM (GA-QPM)^[45]. In addition to QPM in standard PPLN devices mentioned, other approaches for phase matching in TFLN waveguides can simplify their fabrication and device preparation because of the poling-free implementations.

An example of such devices in a rotational symmetry Z-cut TFLN microring is shown in Fig. 3(a), which can be periodically poled by an external electric field between the bottom aluminium plate electrode and the top radial nickel electrodes. Due to the stronger mode confinement of the microring and the phase matching in the periodic domain structure, the QPM SHG conversion efficiency for the periodically poled microring can yield up to $250,000\% \text{W}^{-1}$ ^[46]. Figure 3(b) displays two distinct schemes to achieve the phase-matching condition. Both fixed-width LN waveguides (modal phase matching) and periodically grooved LN (PGLN) waveguides (QPM) were fabricated on an X-cut LNOI platform, which were adopted to realize phase-matched SHG conversion efficiencies of $6.8\% \text{W}^{-1} \text{cm}^{-2}$ and $41\% \text{W}^{-1} \text{cm}^{-2}$, respectively^[44]. To overcome careful dispersion engineering of traditional nonlinear phase matching, Wang *et al.* have demonstrated phase-matching-free SHG over many coherent lengths in TFLN waveguides and that gradient metasurface-based device can maintain a high efficiency over a broad range of pump wavelengths due to the strong nonlinear modal overlap^[47] [see in Fig. 3(c)]. In terms of poling-free methods for SHG in the TFLN platform, employing a sinusoidal width perturbation of the rib-loaded waveguides with silicon nitride (SiN) can achieve GA-QPM based on TFLN [Fig. 3(d)]. The SHG conversion

efficiency is $\sim 1\% \text{W}^{-1} \text{cm}^{-2}$ from 4.9-mm-long waveguides pumped at a 784 nm wavelength. An optimized width modulation pattern and a higher-refractive-index rib material can increase the conversion efficiency of such devices^[45].

Due to a well-designed grating metasurface in the LN slab waveguides to fulfill the phase-matching condition rather than using previous poling technology, SHG and nonlinear beam shaping have been experimentally observed, but the total efficiency has been decreased to 4.6×10^{-7} ^[48]. Furthermore, the detailed comparisons between these TFLN photonics based on waveguides and their corresponding metrics are illustrated in Table 1.

In conclusion, the limitation on poling period is taken into consideration for the optimization of the waveguide to obtain higher nonlinear conversion efficiency, because the required poling period for tightly confined modes in TFLN nanowaveguides will be very small for the required QPM. However, based on waveguide-width modulation or mode-shape modulation being studied, poling-free QPM in TFLN to achieve SHG without periodical poling is obtained^[45]. There is no need to meet the strict phase-matching conditions for TFLN nanostructures in the nonlinear process, which will be discussed clearly in the next section.

2.2. Second harmonic generation in resonant nanostructures

Aside from the applications of PPLN waveguides, TFLN is also a promising candidate to achieve SHG from resonant nanostructures^[49]. Up to now, more and more studies have been performed on TFLN nanostructures. The nanostructures

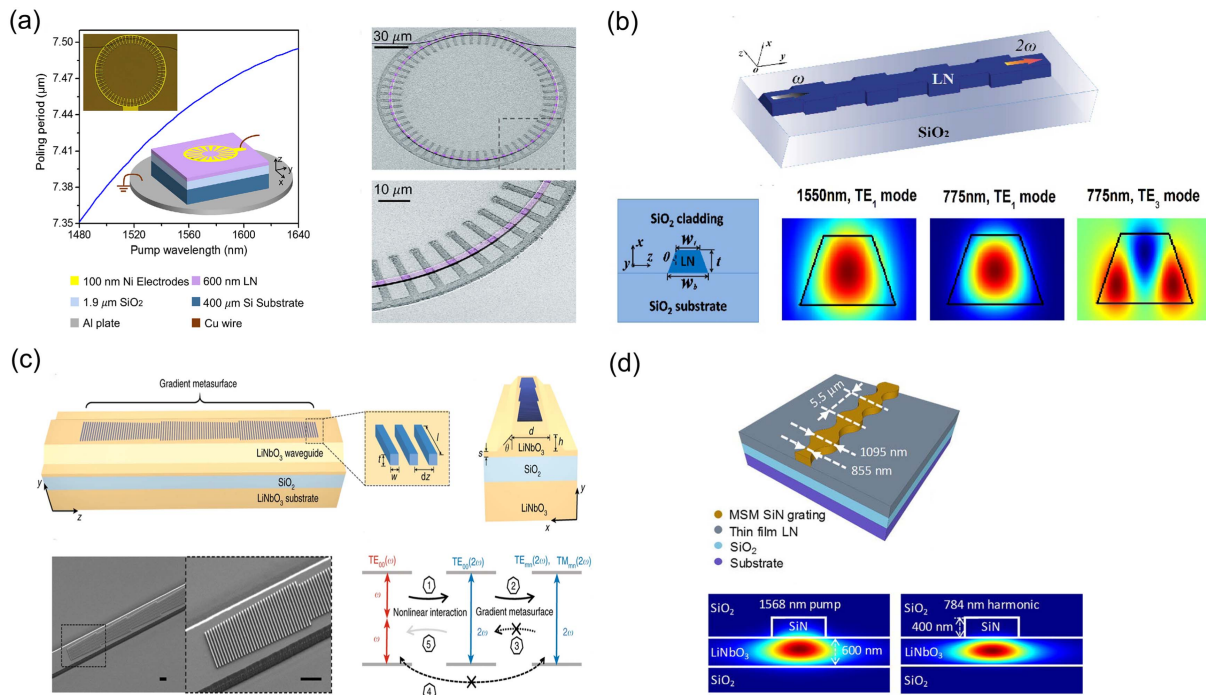


Fig. 3. (a) Demonstration of efficient SHG in PPLN microring resonators^[46]; Copyright 2019, Optical Society of America. (b) Schematic of the periodically grooved structure of an LN waveguide and cross-section image of the X-cut LN waveguide^[44]; Copyright 2017, Optical Society of America. (c) Schematic and working principle of the metasurface-assisted LN nanophotonic waveguide^[47]; Copyright 2017, Springer Nature. (d) Schematic of a rib-loaded GA-QPM waveguide with a sinusoidal modulation of the width along with the optical mode profiles of the fundamental and SH TE modes at a grating width of 1095 nm^[45]; Copyright 2017, AIP Publishing.

different from waveguides have sizes smaller than the coherence length, and there is no need to consider their phase matching. Consequently, phase-matching techniques are not necessary. The recent experiment that applied LN nanocrystal powder as the random scattering medium can achieve the cavity-enhanced SHG process, which has broken phase-matching limitation due to random QPM (RQPM) [see in Fig. 4(a)], and important progress on the Anderson localization of the nonlinear signals has been indicated^[50]. Furthermore, the light field is localized on micro- and nanostructures, which can be exploited in micro-nano photonics devices. It is very suitable for realizing many nonlinear optical frequency conversion effects. Nanostructures can locally confine electromagnetic fields due to their small size and resonant design. This confinement corresponds to resonances that occur at specific wavelengths that can be tuned by changing the size, shape, and material. On the other hand, electric and magnetic resonances and their interference in high-index dielectric nanostructures strongly influence the enhancement of the nonlinear optical interactions. As shown in Fig. 4(b), LN nanocubes with sizes from 200 to 300 nm presented by Timpu *et al.* are all-dielectric Mie-type nanoresonators to obtain strong SHG emission for the near ultraviolet (NUV) range^[51].

Because square-shaped nanoresonators can maximize the amount of the nonlinear material, metasurfaces based on densely packed arrangements of such nanoresonators can be used to realize enhanced optical nonlinearities. Figure 5(a)

demonstrates the resonant enhancement of SHG via Mie-type resonances at a pump wavelength around 1550 nm experimentally, and the SHG signal can be emitted in the zeroth diffraction order normal to the metasurface^[52]. Meanwhile, LN nanograting metasurfaces with controllable SHG properties have been experimentally demonstrated to enhance second harmonic (SH) signals via electric- and magnetic-natured Mie resonances [Fig. 5(b)]. Furthermore, the SHG efficiency spectra can be tuned by changing the geometric parameters^[53].

To realize strong local field confinement at subwavelength volumes, nanoscale resonators such as metallic nanostructures^[54] exploiting plasmonic resonances are required^[55–57]. Moreover, resonant metallic nanostructures simply placed on top of a nonlinear material can provide an enhanced nonlinear response^[58]. Due to the pronounced plasmonic field enhancement, plasmonic nanorings have the unique advantage for highly efficient SHG. Figure 6(a) shows metallic nanorings filled with crystalline LN as a nano-optical device to enhance SHG at NIR frequencies. At normal incidence, measurements and simulations confirm the SH enhancement of about 20^[59]. In order to make meaningful comparisons between optical and plasmonic nonlinear effects, while pumped at a 1240 nm wavelength, the sample consisting of a thin gold film on LN [Fig. 6(b)] can obtain the non-phase-matched SHG response at a gold/air interface to calibrate the plasmonic signal. Phase matching needs to achieve efficient nonlinear conversion in

Table 1. Comparisons of SHG Conversion Efficiency of Different TF-PPLN Waveguides.

Year	TFLN Structure	Poled/Coupling Region Length L (mm)	FF Power (λ_{FF})	Coupling Loss (dB/facet)	Waveguide Propagation Loss (dB/cm)	η_{SH} [% $W^{-1} cm^{-2}$]	Institute
2011	Plasmonic waveguide ^[60]	1	1 W (1550 nm)	-	-	1.3%	Nanjing University
2015	Nanoscale LN waveguides ^[61]	0.9	737 μ W (1411 nm)	-	61	6.9	Friedrich Schiller Universität Jena
2017	PE channel waveguide ^[36]	3.2	1 mW (1385 nm)	-	2.5	48	Shandong University
2016	Rib-loaded SiN-PPLN ^[22]	4.8	0.5 mW (1530 nm)	\sim 6.8	0.3 ± 0.2	160	University of California
2017	Metasurface-assisted PM LN waveguide ^[47]	0.019	10^9 V/m/20 mW (1640 nm)	-	-	1660	Harvard University
2017	GA-QPM LN ridge waveguide ^[45]	4.9	84 mW (1568 nm)	6.5	1	0.8	University of Central Florida
2017	Integrated TFLN waveguide ^[44]	3	18.3 μ W (1550 nm)	4.8	3 ± 0.2	41	Harvard University
2016	Diced ridge PPLN waveguides ^[62]	5.8	6.6 mW (1550 nm)	-	0.57	77.9	Shandong University
2018	PPLN on silicon ^[63]	20	10 mW (1547 nm)	-	0.2	1230	University of Central Florida
2018	Nanostructured PPLN waveguide ^[39]	4	220 mW (1550 nm)	\sim 10	-	2600	Harvard University
2018	LN nanophotonic waveguide ^[64]	8	\sim 1 mW (1540 nm)	5	0.54	22.2	University of Rochester
2019	PPLN microrings ^[46]	-	115 μ W (1617 nm)	-	-	250,000%/W	Yale University
2019	PPLNOI ridge waveguide ^[41]	10	10 mW (1590 nm)	-	-	0.04	Shanghai Jiao Tong University
2019	Dry-etched ^[65]	0.6	1 mW (1540 nm)	6	3	4600	University of Central Florida
2019	Dry-etched ^[21]	4	2.95 mW (1550 nm)	4.3	0.3	2200	Stevens Institute of Technology
2020	Z-cut PPLNOI waveguide ^[66]	1	- (1550 nm)	5.4 ± 0.3	< 0.03	2400	Stevens Institute of Technology
2020	Dry-etched PPLN ^[67]	5	0.1 mW (1570 nm)	-7	-0.54	2000	University of California
2020	PPLNOI ridge waveguide ^[40]	6	397 μ W (1470 nm)	-	-	3061	Nanjing University+Sun Yat-sen University
2020	Birefringent phase-matching LN waveguide ^[68]	10	4500 W (1064 nm)	-	0.58	0.87%	Shandong University

(Continued)

Table 1. (Continued)

Year	TFLN Structure	Poled/Coupling Region Length L (mm)	FF Power (λ_{FF})	Coupling Loss (dB/facet)	Waveguide Propagation Loss (dB/cm)	η_{SH} (% $W^{-1} cm^{-2}$)	Institute
2020	Shallow-etched TFLN waveguides ^[42]	5	10 mW (1560 nm)	7.7	1	3757	University of California
2020	PPLN waveguide ^[69]	6	60 fJ (2050 nm)	-	< 0.1	1000	Stanford University
2020	LN slab waveguides by grating metasurfaces ^[48]	0.05	25 mW (1064 nm)	-	-	4.6×10^{-7}	Nanjing University

plasmonic nanostructures owing to the nature of the nonlinearity, the plasmonic dispersion, and the lower dimensionality of the propagation^[70].

Therefore, free from phase-matching constraints, dielectric nanostructures have contributed significantly to the control of optical nonlinearity and enhancement of nonlinear generation efficiency by engineering subwavelength structures. In addition, it is of high interest to achieve on-chip LNOI microdisk resonators with high- Q factors^[71,72], which may need phase-matching conditions to realize nonlinear effects^[73]. Specially, by combining a 16 μm PPLN with microdisk cavities on a chip, the nonlinear optical performance was then investigated by optimizing the period and pattern of the poled structure and by improving the cavity Q factors (6.7×10^5). From this result, the SHG conversion efficiency can also be significantly improved by on-chip PPLN microcavities^[74]. Then, as seen in Fig. 7(a), both SHG and spontaneous parametric down conversion with a bandwidth over 400 nm on chip can be demonstrated by a high- Q

(1.2×10^5) X-cut LN microdisk resonator, which has a radius of 45 μm and a thickness of 300 nm^[75]. High- Q TFLN microresonators provide an ideal platform for on-chip nonlinear optical applications^[74-76]. Due to the strong nonlinear effects in a photonic molecule (PM) structure composed of two strongly coupled LN microdisks with Q factors as high as 5.1×10^6 (at 1565.46 nm), which can enable phase matching, more nonlinear optical phenomena including cascaded four-wave mixing and stimulated Raman scattering were observed around the SH signal [Fig. 7(b)]^[77]. An X-cut LN microdisk resonator with a diameter of 30 μm , featuring Q factors as high as 9.61×10^6 (at 1547.8 nm), has been used to generate the SH and cascaded third-harmonic waves simultaneously. Using this device, the sign of the effective nonlinear coefficient inverts periodically as light propagates along the microdisk periphery, facilitating QPM without the necessity of domain engineering, as shown in Fig. 7(c). Hence, ultrahigh efficiencies over the broad wavelength range have been realized in nonlinear processes^[78]. As

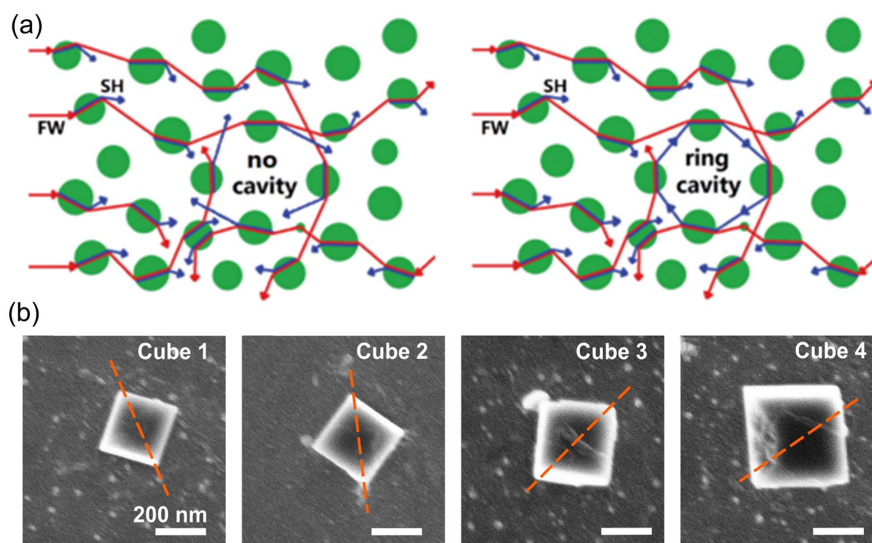


Fig. 4. (a) Schematic of the LN powder to form the cavity behavior in the SH emission at a certain pump intensity^[50], Copyright 2019, American Physical Society. (b) SEM images of single LN nanocubes to obtain the maximal SHG^[51], Copyright 2019, American Chemical Society.

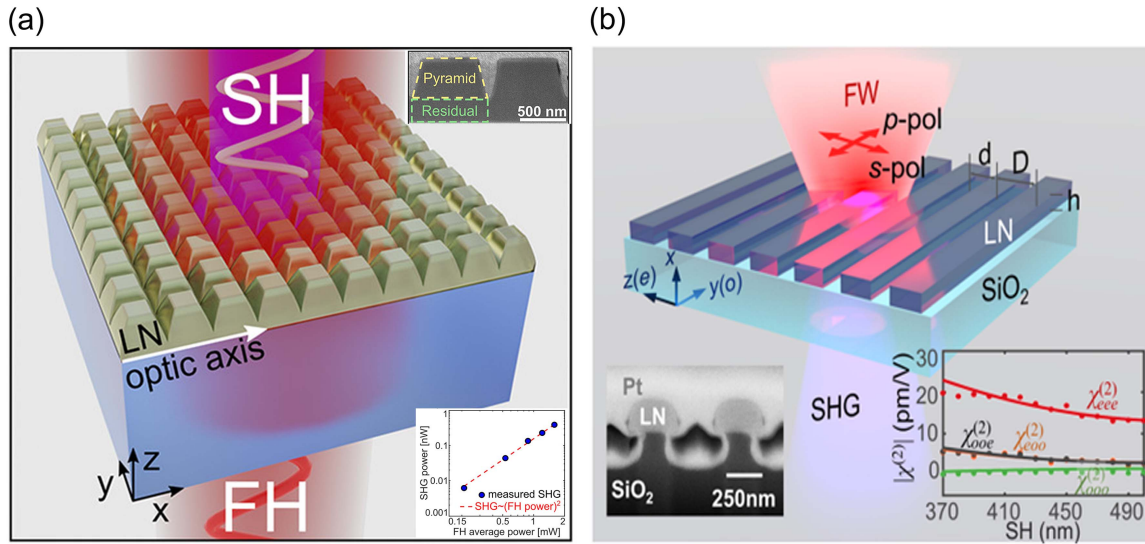


Fig. 5. (a) Images of SHG in an LN metasurface and SHG power depending on average power of the fundamental harmonic (FH) beam^[52]; Copyright 2020, American Chemical Society. (b) Schematic of LN nonlinear metasurfaces fabricated on an X-cut LN film residing on a fused quartz substrate. Left inset gives a typical SEM image of the cross section of the metasurface, and the right inset presents the measured second-order susceptibility of the LN film used in this study^[53]; Copyright 2021, John Wiley and Sons.

such, the TFLN microresonators have been a promising method to promote the performance of current integrated nonlinear photonics to a large extent.

More recently, research on non-radiating electromagnetic states such as the anapole mode^[79,80] is under active study, in particular, at optical wavelengths. Such an interest has been boosted by many studies of light-matter interactions in resonant nanostructures. For example, LN nanodisks placed on aluminum substrates can be theoretically demonstrated to achieve efficient vacuum ultraviolet (VUV) radiation with an efficiency

higher than $10^{-2}\%$, assisted by anapole resonance at the pump wavelength^[81]. The results obtained in this field very recently revealed that this platform allows creating field confinement in high-index contrast nanostructures. Based on this rapidly growing technology, the nanoparticles with moderate refractive indices can generate anapole modes with a highly enhanced near field when they are supported by metallic or near-zero-index substrates. By utilizing the higher index contrast between LN and hyperbolic metamaterial (HMM) with low losses, Li *et al.* have demonstrated record-high 10^{-4} normalized efficiency

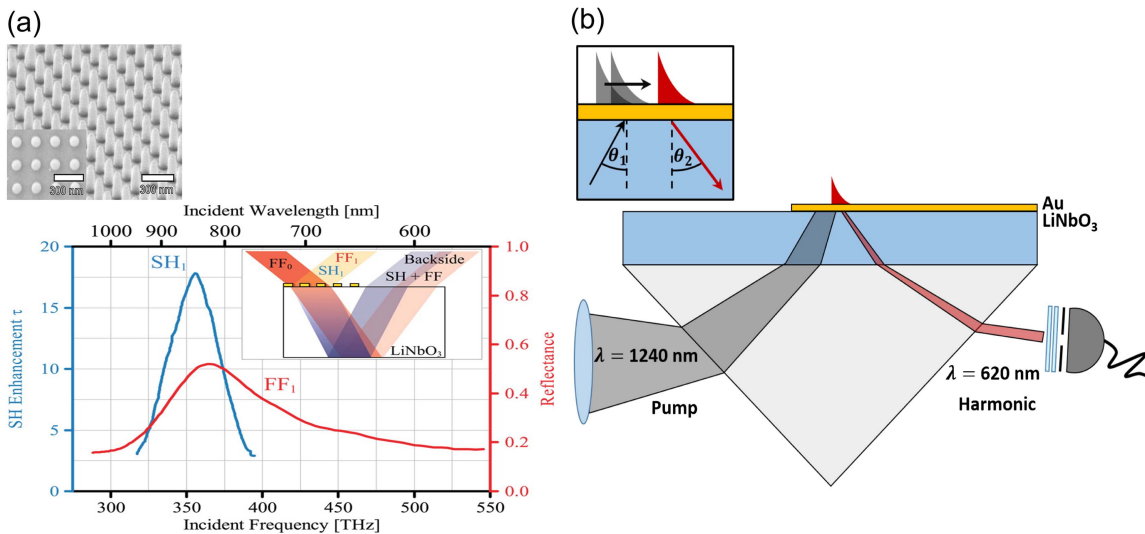


Fig. 6. (a) SEM images showing the mask for ion-beam-enhanced etching (IBEE) (Cr/SiO₂ pillars) and measured SH enhancement factor and linear reflection spectrum of the fabricated sample^[59]; Copyright 2015, American Chemical Society. (b) Schematic of the experiment mounted using index matching oil in a typical Kretschmann geometry^[70]; Copyright 2018, Optical Society of America.

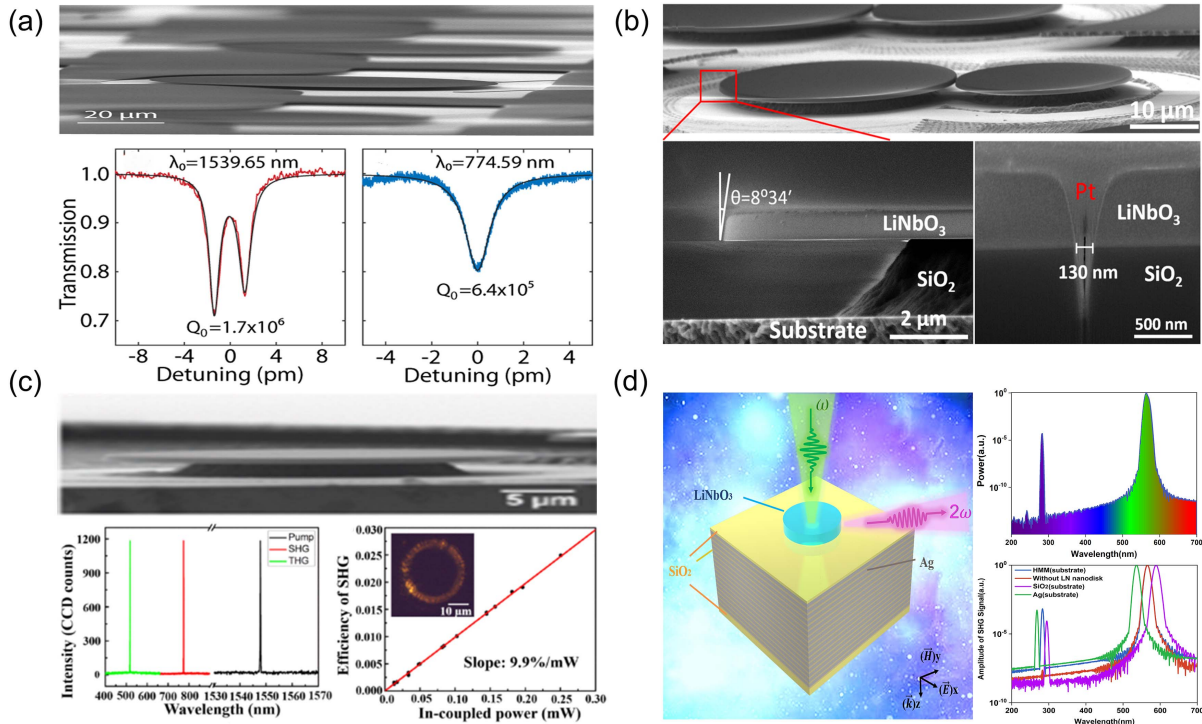


Fig. 7. (a) Scanning-electron micrograph of LN microresonators to achieve modal dispersion^[75]; Copyright 2017, Optical Society of America. (b) SEM images of the LN microdisk PM^[77]; Copyright 2020, IOP Publishing. (c) SEM image of the X-cut LN microdisk and spectra of the pump light, the second-harmonic wave, and the third-harmonic wave. SHG conversion efficiency as a function of the in-coupled power^[78]; Copyright 2019, American Physical Society. (d) Schematic depiction of the proposed nanostructure for generating SH and nonlinear simulations^[82]; Copyright 2020, De Gruyter.

Table 2. Performance Comparisons of Different Micro- and Nanostructures Based on TFLN.

Year	Structure	Mechanism	Structure Parameter (Radius R , Diameter D , Height H , Thickness T)	Peak Pump Intensity/Power (λ_{PF})	Q Factor (λ)	η_{SH}	$\eta_{\text{dim}}^{\text{SH}}$ (W^{-1})/Unstructured LN	Institute
2012–2013	Embedded Ag-LN ^[83,84]	Fabry-Perot resonance	Coaxial aperture ($R_{\text{inner}} = 65 \text{ nm}$, $R_{\text{outer}} = 135 \text{ nm}$, $H = 120 \text{ nm}$)	– 1550 nm	–	–	~27 times	FEMTO-ST, CNRS
2014	LN microdisk resonators ^[85]	Cavity resonance	LN microdisk ($D = 28 \text{ }\mu\text{m}$, $T = \sim 300 \text{ nm}$)	1.8 mW (1546 nm)	1.02×10^5 (1507 nm)	–	0.109	Harvard University
2015	High- Q LN microresonator ^[76]	Femtosecond laser micromachining	LN microdisk ($D = \sim 82 \text{ }\mu\text{m}$, $T = \sim 670 \text{ nm}$)	54.6 μW (1550 nm)	2.45×10^6 (1550 nm)	–	2.30×10^{-3}	Shanghai Institute of Optics and Fine Mechanics
2015	LN-filled gold nanorings ^[59]	Plasmonic resonance	Ring $R_{\text{inner}} = 80 \text{ nm}$, $R_{\text{outer}} = 120 \text{ nm}$, $H = 100 \text{ nm}$	4 GW/cm^2 (820 nm)	–	–	~20 times	Friedrich Schiller University Jena
2017	LN microdisk resonator ^[75]	Broadband SPDC	LN microdisk ($R = 45 \text{ }\mu\text{m}$, $T = 300 \text{ nm}$)	115 μW (1549.32 nm)	1.2×10^5 (1549.32 nm)	–	3.6×10^{-3}	University of Rochester

(Continued)

Table 2. (Continued)

Year	Structure	Mechanism	Structure Parameter (Radius R , Diameter D , Height H , Thickness T)	Peak Pump Intensity/ Power (λ_{FP})	Q Factor (λ)	η_{SH}	$\eta_{\text{dim}}^{\text{SH}}$ (W^{-1})/ Unstructured LN	Institute
2018	PPLN microcavity ^[74]	Whispering gallery mode (WGM)	PPLN microdisk ($D = \sim 80 \mu\text{m}$, $T = 700 \text{ nm}$)	1.1 mW (1550 nm)	6.7×10^5	-	2.2×10^{-3}	Nankai University
2018	Gold deposited on TFLN ^[70]	Plasmonic SHG	Gold film ($T = \sim 30 \text{ nm}$)	60 MW/cm ² (1240 nm)	-	2×10^{-13}	-	Macquarie University
2018	LN nanodisks on an Al substrate ^[81]	Anapole resonances	LN nanodisk ($D = 256 \text{ nm}$, $H = 70 \text{ nm}$)	5.31 GW/cm ² (351.3 nm)	-	1.1528×10^{-5}	-	Institute of Lasers, State Academy of Sciences
2019	On-chip monocrystalline TFLN microdisk resonator ^[78]	QPM	LN microdisk ($D = \sim 30 \mu\text{m}$, $T = 600 \text{ nm}$)	0.25 mW (1547.8 nm)	9.61×10^6 (1547.8 nm)	-	9.9%/mW	Shanghai Institute of Optics and Fine Mechanics
2019	LNO nanocubes ^[51]	Mie resonances	Nanocube (200 nm)	1.7 GW/cm ² (720 nm)	-	-	7.6×10^{-7}	ETH Zürich
2019	Periodic LN bar and LN disk ^[24]	Fano resonances	Bar and disk ($D = 700 \text{ nm}$, $T = 340 \text{ nm}$, $L = 1100 \text{ nm}$)	3.2 GW/cm ² (1605 nm)	2350 (1605 nm)	3.165×10^{-4}	-	Jinan University
2019	Superfine LN powder ^[50]	Cavity-enhanced SHG	-	1.58 GW/cm ² (793.5 nm)	-	-	-	Shanghai Jiao Tong University
2020	BPPLN microcavities ^[49]	Multiple reciprocal vectors	Minimum domain unit (width = 100 nm)	0.02 mW (1550 nm)	1.43×10^5	-	5.1×10^{-1}	Nankai University
2020	LNOI wafer ^[86]	Fabry-Perot resonance	LN film ($H = 196.8 \text{ nm}$)	4.05 GW/cm ² (840 nm)	-	1.6×10^{-5}	-	Nankai University
2020	Nanostructured LN ^[82]	Anapole resonances	LN nanodisk ($D = 432 \text{ nm}$, $H = 104 \text{ nm}$)	5.31 GW/cm ² (565.4 nm)	-	5.1371×10^{-5}	0.1711	Jinan University
2020	LN metasurface ^[52]	ED and MD Mie resonances	Nanocube (period = 870 nm, length = 700 nm)	4.3 GW/cm ² (1550 nm)	-	$\sim 10^{-6}$	1.14×10^{-3}	Friedrich Schiller University Jena
2021	LN nanograting metasurfaces ^[83]	Mie resonance	Metasurface (period $D = 600 \text{ nm}$, $H = 235 \text{ nm}$)	2.05 GW/cm ² (820 nm)	-	4.2×10^{-6}	~ 2 times	Nankai University
2021	Integrated LN microresonators ^[87]	Ultrahigh Q performance	LN microdisk ($D = 1030 \mu\text{m}$)	5 μW (1550 nm)	1.56×10^8 ($\sim 1551.52 \text{ nm}$)	-	602%/mW	Shanghai Institute of Optics and Fine Mechanics

under pump intensity of 11 GW/cm^2 via anapole excitation, as shown in Fig. 7(d). The design of the mentioned configuration can be tuned by tailoring the geometric parameters of the nanostructure to achieve an enhanced and flexible SHG^[82].

In addition to the resonances mentioned above, Huang *et al.* reported that highly efficient TFLN periodic nanostructures assisted by Fano resonance with the Q of 2350 (at 1605 nm) in 2019^[24] have also showed a large SH enhancement and yielded a higher SH conversion efficiency. Further studies on the EO effect in LN can achieve a tunable SHG with voltage excitations. Other research groups have also demonstrated various methods for nanostructures to excite a high field confinement of the different resonances to obtain higher nonlinear conversion efficiency^[49–59,70–76,85,87,88].

This section aims to provide a brief review of the key advances on SHG processes in TFLN micro- and nanostructures, concentrating on four important structures, namely nanoparticles, metasurfaces, plasmonics, and micro- and nanodisks. Different from the structured waveguides, these resonant structures have compact size and field confinement for nonlinear optical properties. The micro- and nanostructures based on TFLN technology introduced here, but not limited to these, will together pave the way to a wide range of functional devices and promising applications. Meanwhile, many ingenious methods for TFLN nanostructures with higher SHG conversion efficiency are also summarized in Table 2.

To date, improvements in optical efficiency have been realized in nonlinear optics supported by technologies of TFLN nanostructures. The growing activities and the great potential of TFLN-based devices will lead to novel concepts and architectures of high-performance integrated optics with highly efficient nonlinear optical devices.

3. Conclusions and Perspectives

In summary, we have profoundly reviewed and discussed the recent progress in the intensely developing area of nonlinear waveguides and nanostructures made by TFLN to increase the SHG efficiency. First, the brief introduction of the rapid developments of SHG and TFLN material are demonstrated. What follows is the key section of this review, which, respectively, presents the comprehensive analyses of the waveguide and nanostructure to achieve high SHG efficiency. The SHG conversion efficiency of the structured waveguides and resonant nanostructures is approaching $\eta_{\text{SH}} \sim 10^3\% \text{ W}^{-1} \text{ cm}^{-2}$ with lower waveguide propagation loss and $\eta_{\text{dim}}^{\text{SH}} \sim 10^{-1} \text{ W}^{-1}$, respectively. Furthermore, these two kinds of structures have been widely applied in nonlinear optics and proven invaluable in the development of future nonlinear integrated photonics. Finally, the future perspectives and main challenges of TFLN nonlinear integrated photonics are discussed. It is important to mention that TFLN is a promising material to enhance light-matter interactions, whose integration helps improve the performances of LN photonic devices.

Further, though much smaller poling periods are required for the PPLN approaches, many TFLN integrated waveguide devices are mature for industrial implementation. In fact, a thorough study needs to be done to make TFLN an attractive and competitive integrated nonlinear optical platform. The large-scale fabrication of high- Q TFLN structures and their integration with photonics devices still require suitable advanced production tools and relevant infrastructures. However, to utilize the remarkable optical properties of the TFLN material to the largest extent, various types of waveguides and nanostructures need to be carefully and properly designed to further optimize the nonlinear optical performances of TFLN devices, considering the underlying compatible technologies. Thus, it can be concluded that integrated TFLN-based nonlinear nanophotonics are still a rapidly developing platform, and more excellent optical properties need to be studied in this platform. This will pave the way for technological development and industrialization of high-performance TFLN integrated photonics in the future.

Overall, there are various potential applications for booming TFLN-based nonlinear devices to overcome the challenges of TFLN from design, fabrication, and practical application in recent years. These can greatly inspire advancements in different kinds of fields, such as lasers, quantum communications, optical communications, imaging, optical memories, and diffractive optics.

Acknowledgement

This work was supported by the National Natural Science Foundation of China (Nos. 61775084, 61705089, 61705087, 62075088, and 61505069), NSAF (No. U2030103), Guangdong Special Support Program (No. 2016TQ03X962), Natural Science Foundation of Guangdong Province (Nos. 2021A0505030036, 2020A151501791, and 2021A1515011875), Open Fund of Guangdong Provincial Key Laboratory of Information Photonics Technology of Guangdong University of Technology (No. GKPT20-03), and Fundamental Research Funds for the Central Universities (No. 11620444).

References

1. P. A. Franken, A. E. Hill, C. W. Peters, and G. Weinreich, "Generation of optical harmonics," *Phys. Rev. Lett.* **7**, 118 (1961).
2. L. P. Gonzalez, D. C. Upchurch, P. G. Schunemann, L. Mohnkern, and S. Guha, "Second-harmonic generation of a tunable continuous-wave CO_2 laser in orientation-patterned GaAs," *Opt. Lett.* **38**, 320 (2013).
3. Y. Liu, X. Yan, J. Wu, B. Zhu, Y. Chen, and X. Chen, "On-chip erbium-doped lithium niobate microcavity laser," *Sci. Chin. Phys. Mech. Astron.* **64**, 234262 (2020).
4. S. V. Makarov, M. I. Petrov, U. Zywiets, V. Milichko, D. Zuev, N. Lopanitsyna, A. Kuksin, I. Mukhin, G. Zograf, E. Ubyivovk, D. A. Smirnova, S. Starikov, B. N. Chichkov, and Y. S. Kivshar, "Efficient second-harmonic generation in nanocrystalline silicon nanoparticles," *Nano Lett.* **17**, 3047 (2017).
5. Y. Qiao, Y. Peng, Y. Zheng, F. Ye, and X. Chen, "Second-harmonic focusing by a nonlinear turbid medium via feedback-based wavefront shaping," *Opt. Lett.* **42**, 1895 (2017).

6. M. Yu, L. Shao, Y. Okawachi, A. L. Gaeta, and M. Loncar, "Ultraviolet to mid-infrared supercontinuum generation in lithium-niobate waveguides," in *CLEO: Science and Innovations* (2020), paper STu4H. 1.
7. M. Yu, B. Desiatov, Y. Okawachi, A. L. Gaeta, and M. Loncar, "Coherent two-octave-spanning supercontinuum generation in lithium-niobate waveguides," *Opt. Lett.* **44**, 1222 (2019).
8. A. Sergeev, R. Geiss, A. S. Solntsev, A. Steinbruck, F. Schrepel, E. B. Kley, T. Pertsch, and R. Grange, "Second-harmonic generation in lithium niobate nanowires for local fluorescence excitation," *Opt. Express* **21**, 19012 (2013).
9. N. C. Panoiu, W. E. I. Sha, D. Y. Lei, and G. C. Li, "Nonlinear optics in plasmonic nanostructures," *J. Opt.* **20**, 083001 (2018).
10. B. Zhang, L. Wang, and F. Chen, "Recent advances in femtosecond laser processing of LiNbO₃ crystals for photonic applications," *Laser Photon. Rev.* **14**, 1900407 (2020).
11. B. Sain, C. Meier, and T. Zentgraf, "Nonlinear optics in all-dielectric nano-antennas and metasurfaces: a review," *Adv. Photon.* **1**, 024002 (2019).
12. H. Lu, H. Xiong, Z. Huang, Y. Li, H. Dong, D. He, J. Dong, H. Guan, W. Qiu, X. Zhang, W. Zhu, J. Yu, Y. Luo, J. Zhang, and Z. Chen, "Electron-plasmon interaction on lithium niobate with gold nanolayer and its field distribution dependent modulation," *Opt. Express* **27**, 19852 (2019).
13. A. Rao and S. Fathpour, "Heterogeneous thin-film lithium niobate integrated photonics for electrooptics and nonlinear optics," *IEEE J. Sel. Top. Quantum Electron.* **24**, 8200912 (2018).
14. C. Pang, R. Li, Z. Li, N. Dong, F. Ren, J. Wang, and F. Chen, "A novel hierarchical nanostructure for enhanced optical nonlinearity based on scattering mechanism," *Small* **16**, 2003172 (2020).
15. Y. Jia, L. Wang, and F. Chen, "Ion-cut lithium niobate on insulator technology: recent advances and perspectives," *Appl. Phys. Rev.* **8**, 011307 (2021).
16. M. Levy, R. M. Osgood, R. Liu, L. E. Cross, G. S. Cargill, A. Kumar, and H. Bakhru, "Fabrication of single-crystal lithium niobate films by crystal ion slicing," *Appl. Phys. Lett.* **73**, 2293 (1998).
17. A. Honardoost, K. Abdelsalam, and S. Fathpour, "Rejuvenating a versatile photonic material: thin-film lithium niobate," *Laser Photon. Rev.* **14**, 2000088 (2020).
18. P. Rabiei and P. Gunter, "Optical and electro-optical properties of submicrometer lithium niobate slab waveguides prepared by crystal ion slicing and wafer bonding," *Appl. Phys. Lett.* **85**, 4603 (2004).
19. B. Zhu, H. Liu, Y. A. Liu, X. Yan, Y. Chen, and X. Chen, "Second-harmonic computer-generated holographic imaging through monolithic lithium niobate crystal by femtosecond laser micromachining," *Opt. Lett.* **45**, 4132 (2020).
20. G. T. Reed, G. Z. Mashanovich, F. Y. Gardes, M. Nedeljkovic, Y. Hu, D. J. Thomson, K. Li, P. R. Wilson, S.-W. Chen, and S. S. Hsu, "Recent breakthroughs in carrier depletion based silicon optical modulators," *Nanophotonics* **3**, 229 (2014).
21. J.-Y. Chen, Y. M. Sua, Z.-H. Ma, C. Tang, Z. Li, and Y.-P. Huang, "Efficient parametric frequency conversion in lithium niobate nanophotonic chips," *OSA Continuum* **2**, 2914 (2019).
22. L. Chang, Y. Li, N. Volet, L. Wang, J. Peters, and J. E. Bowers, "Thin film wavelength converters for photonic integrated circuits," *Optica* **3**, 531 (2016).
23. T. J. Kippenberg, R. Holzwarth, and S. A. Diddams, "Microresonator-based optical frequency combs," *Science* **332**, 555 (2011).
24. Z. Huang, H. Lu, H. Xiong, Y. Li, H. Chen, W. Qiu, H. Guan, J. Dong, W. Zhu, J. Yu, Y. Luo, J. Zhang, and Z. Chen, "Fano resonance on nanostructured lithium niobate for highly efficient and tunable second harmonic generation," *Nanomaterials* **9**, 69 (2019).
25. D. Smirnova, A. I. Smirnov, and Y. S. Kivshar, "Multipolar second-harmonic generation by Mie-resonant dielectric nanoparticles," *Phys. Rev. A* **97**, 013807 (2018).
26. N. Yao, J. Zhou, R. Gao, J. Lin, M. Wang, Y. Cheng, W. Fang, and L. Tong, "Efficient light coupling between an ultra-low loss lithium niobate waveguide and an adiabatically tapered single mode optical fiber," *Opt. Express* **28**, 12416 (2020).
27. J. Lin, F. Bo, Y. Cheng, and J. Xu, "Advances in on-chip photonic devices based on lithium niobate on insulator," *Photon. Res.* **8**, 1910 (2020).
28. M. Bazzan and C. Sada, "Optical waveguides in lithium niobate: recent developments and applications," *Appl. Phys. Rev.* **2**, 040603 (2015).
29. W. J. Park, W. S. Yang, W. K. Kim, H. Y. Lee, J. W. Lim, M. Isshiki, and D. H. Yoon, "Ridge structure etching of LiNbO₃ crystal for optical waveguide applications," *Opt. Mater.* **28**, 216 (2006).
30. R. Wolf, I. Breunig, H. Zappe, and K. Buse, "Cascaded second-order optical nonlinearities in on-chip micro rings," *Opt. Express* **25**, 29927 (2017).
31. L. Ariztendi, "Photonic applications of lithium niobate crystals," *Phys. Status Solidi (A)* **201**, 253 (2004).
32. R. W. Boyd, *Nonlinear Optics* (Elsevier, 2003).
33. S. Fathpour, "Heterogeneous nonlinear integrated photonics," *IEEE J. Quantum Electron.* **54**, 6300716 (2018).
34. J. A. Armstrong, N. Bloembergen, J. Ducuing, and P. S. Pershan, "Interactions between light waves in a nonlinear dielectric," *Phys. Rev.* **127**, 1918 (1962).
35. J. E. Toney, *Lithium Niobate Photonics* (Artech House, 2015).
36. L. Cai, Y. Wang, and H. Hu, "Efficient second harmonic generation in $\chi^{(2)}$ profile reconfigured lithium niobate thin film," *Opt. Commun.* **387**, 405 (2017).
37. J. Webjörn, D. Nam, S. Siala, and R. Waarts, "Nonlinear waveguides on the way to the marketplace," *Opt. Photon. News* **8**, 16 (1997).
38. Y. Qi and Y. Li, "Integrated lithium niobate photonics," *Nanophotonics* **9**, 1287 (2020).
39. C. Wang, C. Langrock, A. Marandi, M. Jankowski, M. Zhang, B. Desiatov, M. M. Fejer, and M. Loncar, "Ultra-high-efficiency wavelength conversion in nanophotonic periodically poled lithium niobate waveguides," *Optica* **5**, 1438 (2018).
40. Y. Niu, C. Lin, X. Liu, Y. Chen, X. Hu, Y. Zhang, X. Cai, Y.-X. Gong, Z. Xie, and S. Zhu, "Optimizing the efficiency of a periodically poled LNOI waveguide using *in situ* monitoring of the ferroelectric domains," *Appl. Phys. Lett.* **116**, 101104 (2020).
41. T. Ding, Y. Zheng, and X. Chen, "Integration of cascaded electro-optic and nonlinear processes on a lithium niobate on insulator chip," *Opt. Lett.* **44**, 1524 (2019).
42. J. Zhao, M. Rüsing, U. A. Javid, J. Ling, M. Li, Q. Lin, and S. Mookherjea, "Shallow-etched thin-film lithium niobate waveguides for highly-efficient second-harmonic generation," *Opt. Express* **28**, 19669 (2020).
43. L. Wang, L.-Q. Li, X.-T. Zhang, and F. Chen, "Type I phase matching in thin film of lithium niobate on insulator," *Res. Phys.* **16**, 103011 (2020).
44. C. Wang, X. Xiong, N. Andrade, V. Venkataraman, X.-F. Ren, G.-C. Guo, and M. Loncar, "Second harmonic generation in nano-structured thin-film lithium niobate waveguides," *Opt. Express* **25**, 6963 (2017).
45. A. Rao, J. Chiles, S. Khan, S. Toroghi, M. Malinowski, G. F. Camacho-González, and S. Fathpour, "Second-harmonic generation in single-mode integrated waveguides based on mode-shape modulation," *Appl. Phys. Lett.* **110**, 111109 (2017).
46. J. Lu, J. B. Surya, X. Liu, A. W. Bruch, Z. Gong, Y. Xu, and H. X. Tang, "Periodically poled thin-film lithium niobate microring resonators with a second-harmonic generation efficiency of 250,000%/W," *Optica* **6**, 1455 (2019).
47. C. Wang, Z. Li, M.-H. Kim, X. Xiong, X.-F. Ren, G.-C. Guo, N. Yu, and M. Loncar, "Metasurface-assisted phase-matching-free second harmonic generation in lithium niobate waveguides," *Nat. Commun.* **8**, 2098 (2017).
48. B. Fang, H. Li, S. Zhu, and T. Li, "Second-harmonic generation and manipulation in lithium niobate slab waveguides by grating metasurfaces," *Photon. Res.* **8**, 1296 (2020).
49. L. Zhang, Z. Hao, W. Mao, A. Gao, F. Bo, F. Gao, G. Zhang, and J. Xu, "Biperiodically poled lithium niobate microcavities for multiple nonlinear optical processes," in *CLEO: Science and Innovations* (2020), paper JTh2E.17.
50. Y. Qiao, F. Ye, Y. Zheng, and X. Chen, "Cavity-enhanced second-harmonic generation in strongly scattering nonlinear media," *Phys. Rev. A* **99**, 043844 (2019).
51. F. Timpu, J. Sendra, C. Renaut, L. Lang, M. Timofeeva, M. T. Buscaglia, V. Buscaglia, and R. Grange, "Lithium niobate nanocubes as linear and nonlinear ultraviolet Mie resonators," *ACS Photon.* **6**, 545 (2019).
52. A. Fedotova, M. Younesi, J. Sautter, A. Vaskin, F. J. F. Löchner, M. Steinert, R. Geiss, T. Pertsch, I. Staude, and F. Setzpfandt, "Second-harmonic generation in resonant nonlinear metasurfaces based on lithium niobate," *Nano Lett.* **20**, 8608 (2020).
53. J. Ma, M. Ren, W. Wu, W. Cai, and J. Xu, "Resonantly tunable second harmonic generation from lithium niobate metasurfaces," arXiv:2002.06594 (2020).
54. V. F. Gili, L. Ghirardini, D. Rocco, G. Marino, I. Favero, I. Roland, G. Pellegrini, L. Duò, M. Finazzi, L. Carletti, A. Locatelli, A. Lemaître, D. Neshev, C. De Angelis, G. Leo, and M. Celebrano, "Metal-dielectric

- hybrid nanoantennas for efficient frequency conversion at the anapole mode," *Beilstein J. Nanotechnol.* **9**, 2306 (2018).
55. G. Grinblat, M. Rahmani, E. Cortés, M. Caldarola, D. Comedi, S. A. Maier, and A. V. Bragas, "High-efficiency second harmonic generation from a single hybrid ZnO nanowire/Au plasmonic nano-oligomer," *Nano Lett.* **14**, 6660 (2014).
 56. M. Mayy, G. Zhu, A. Webb, H. Ferguson, T. Norris, V. Podolskiy, and M. Noginov, "Toward parametric amplification in plasmonic systems: second harmonic generation enhanced by surface plasmon polaritons," *Opt. Express* **22**, 7773 (2014).
 57. B. Metzger, M. Hentschel, M. Lippitz, and H. Giessen, "Third-harmonic spectroscopy and modeling of the nonlinear response of plasmonic nanoantennas," *Opt. Lett.* **37**, 4741 (2012).
 58. D. Bar-Lev and J. Scheuer, "Efficient second harmonic generation using nonlinear substrates patterned by nano-antenna arrays," *Opt. Express* **21**, 29165 (2013).
 59. D. Lehr, J. Reinhold, I. Thiele, H. Hartung, K. Dietrich, C. Menzel, T. Pertsch, E.-B. Kley, and A. Tünnermann, "Enhancing second harmonic generation in gold nanoring resonators filled with lithium niobate," *Nano Lett.* **15**, 1025 (2015).
 60. F. Lu, T. Li, X. Hu, Q. Cheng, S. Zhu, and Y. Zhu, "Efficient second-harmonic generation in nonlinear plasmonic waveguide," *Opt. Lett.* **36**, 3371 (2011).
 61. R. Geiss, S. Saravi, A. Sergeev, S. Diziain, F. Setzpfandt, F. Schrepel, R. Grange, E.-B. Kley, A. Tünnermann, and T. Pertsch, "Fabrication of nanoscale lithium niobate waveguides for second-harmonic generation," *Opt. Lett.* **40**, 2715 (2015).
 62. L. Ai, L. Wang, Y. Tan, S. Akhmedaliev, S. Zhou, and F. Chen, "Efficient second harmonic generation of diced ridge waveguides based on carbon ion-irradiated periodically poled LiNbO₃," *J. Lightwave Technol.* **35**, 2476 (2016).
 63. A. Rao, K. Abdelsalam, T. Sjaardema, G. F. Camacho-González, A. Honardoost, and S. Fathpour, "Highly efficient nonlinear integrated photonics in ultracompact periodically-poled lithium niobate on silicon," in *Frontiers in Optics/Laser Science* (OSA Technical Digest, 2018), paper JTu3A.59.
 64. R. Luo, Y. He, H. Liang, M. Li, and Q. Lin, "Highly tunable efficient second-harmonic generation in a lithium niobate nanophotonic waveguide," *Optica* **5**, 1006 (2018).
 65. A. Rao, K. Abdelsalam, T. Sjaardema, A. Honardoost, G. F. Camacho-Gonzalez, and S. Fathpour, "Actively-monitored periodic-poling in thin-film lithium niobate photonic waveguides with ultrahigh nonlinear conversion efficiency of 4600 % W⁻¹ cm⁻²," *Opt. Express* **27**, 25920 (2019).
 66. J.-Y. Chen, C. Tang, Z.-H. Ma, Z. Li, Y. M. Sua, and Y.-P. Huang, "Efficient and highly tunable second-harmonic generation in Z-cut periodically poled lithium niobate nanowaveguides," *Opt. Lett.* **45**, 3789 (2020).
 67. J. Zhao, C. Ma, M. Rüsing, and S. Mookherjee, "High quality entangled photon pair generation in periodically poled thin-film lithium niobate waveguides," *Phys. Rev. Lett.* **124**, 163603 (2020).
 68. B. Zhang, L. Li, L. Wang, and F. Chen, "Second harmonic generation in femtosecond laser written lithium niobate waveguides based on birefringent phase matching," *Opt. Mater.* **107**, 110075 (2020).
 69. M. Jankowski, C. Langrock, B. Desiatov, A. Marandi, C. Wang, M. Zhang, C. R. Phillips, M. Lončar, and M. M. Fejer, "Ultrabroadband nonlinear optics in nanophotonic periodically poled lithium niobate waveguides," *Optica* **7**, 40 (2020).
 70. V. Ng, A. M. Warrior, J. Lin, D. J. Spence, J. E. Downes, D. W. Coutts, and J. M. Dawes, "Plasmonic second-harmonic generation in gold:lithium niobate thin films," *J. Opt. Soc. Am. B* **35**, 302 (2018).
 71. J. Zhang, Z. Fang, J. Lin, J. Zhou, M. Wang, R. Wu, R. Gao, and Y. Cheng, "Fabrication of crystalline microresonators of high quality factors with a controllable wedge angle on lithium niobate on insulator," *Nanomaterials* **9**, 1218 (2019).
 72. J. Lin, Y. Xu, Z. Fang, M. Wang, J. Song, N. Wang, L. Qiao, W. Fang, and Y. Cheng, "Fabrication of high-Q lithium niobate microresonators using femtosecond laser micromachining," *Sci. Rep.* **5**, 8072 (2015).
 73. J. Lin, Y. Xu, J. Ni, M. Wang, Z. Fang, L. Qiao, W. Fang, and Y. Cheng, "Phase-matched second-harmonic generation in an on-chip LiNbO₃ microresonator," *Phys. Rev. Appl.* **6**, 014002 (2016).
 74. Z. Hao, L. Zhang, A. Gao, W. Mao, X. Lyu, X. Gao, F. Bo, F. Gao, G. Zhang, and J. Xu, "Periodically poled lithium niobate whispering gallery mode microcavities on a chip," *Sci. Chin. Phys. Mech. Astron.* **61**, 114211 (2018).
 75. R. Luo, H. Jiang, S. Rogers, H. Liang, Y. He, and Q. Lin, "On-chip second-harmonic generation and broadband parametric down-conversion in a lithium niobate microresonator," *Opt. Express* **25**, 24531 (2017).
 76. J. Lin, Y. Xu, Z. Fang, M. Wang, N. Wang, L. Qiao, W. Fang, and Y. Cheng, "Second harmonic generation in a high-Q lithium niobate microresonator fabricated by femtosecond laser micromachining," *Sci. Chin. Phys. Mech. Astron.* **58**, 114209 (2015).
 77. M. Wang, N. Yao, R. Wu, Z. Fang, S. Lv, J. Zhang, J. Lin, W. Fang, and Y. Cheng, "Strong nonlinear optics in on-chip coupled lithium niobate microdisk photonic molecules," *New J. Phys.* **22**, 073030 (2020).
 78. J. Lin, N. Yao, Z. Hao, J. Zhang, W. Mao, M. Wang, W. Chu, R. Wu, Z. Fang, L. Qiao, W. Fang, F. Bo, and Y. Cheng, "Broadband quasi-phase-matched harmonic generation in an on-chip monocrystalline lithium niobate microdisk resonator," *Phys. Rev. Lett.* **122**, 173903 (2019).
 79. M. Timofeeva, L. Lang, F. Timpu, C. Renaut, A. Bouravlev, I. Shtrom, G. Cirlin, and R. Grange, "Anapoles in free-standing III-V nanodisks enhancing second-harmonic generation," *Nano Lett.* **18**, 3695 (2018).
 80. K. V. Baryshnikova, D. A. Smirnova, B. S. Luk'yanchuk, and Y. S. Kivshar, "Optical anapoles: concepts and applications," *Adv. Opt. Mater.* **7**, 1801350 (2019).
 81. K.-H. Kim and W.-S. Rim, "Anapole resonances facilitated by high-index contrast between substrate and dielectric nanodisk enhance vacuum ultraviolet generation," *ACS Photon.* **5**, 4769 (2018).
 82. Y. Li, Z. Huang, Z. Sui, H. Chen, X. Zhang, W. Huang, H. Guan, W. Qiu, J. Dong, W. Zhu, J. Yu, H. Lu, and Z. Chen, "Optical anapole mode in nanostructured lithium niobate for enhancing second harmonic generation," *Nanophotonics* **9**, 3575 (2020).
 83. E. Barakat, M.-P. Bernal, and F. I. Baida, "Doubly resonant Ag-LiNbO₃ embedded coaxial nanostructure for high second-order nonlinear conversion," *J. Opt. Soc. Am. B* **30**, 1975 (2013).
 84. E. Barakat, M.-P. Bernal, and F. I. Baida, "Theoretical analysis of enhanced nonlinear conversion from metallo-dielectric nano-structures," *Opt. Express* **20**, 16258 (2012).
 85. C. Wang, M. J. Burek, Z. Lin, H. A. Atikian, V. Venkataraman, I. C. Huang, P. Stark, and M. Lončar, "Integrated high quality factor lithium niobate microdisk resonators," *Opt. Express* **22**, 30924 (2014).
 86. J. Ma, J. Chen, M. Ren, W. Wu, W. Cai, and J. Xu, "Second-harmonic generation and its nonlinear depolarization from lithium niobate thin films," *Opt. Lett.* **45**, 145 (2020).
 87. R. Gao, H. Zhang, F. Bo, W. Fang, Z. Hao, N. Yao, J. Lin, J. Guan, L. Deng, and M. Wang, "Ultrahigh quality-factor microresonators fabricated in pristine lithium niobate thin film for efficient nonlinear optics applications," arXiv:2102.00399 (2021).
 88. J. Ma, F. Xie, W. Chen, J. Chen, W. Wu, W. Liu, Y. Chen, W. Cai, M. Ren, and J. Xu, "Nonlinear lithium niobate metasurfaces for second harmonic generation," *Laser Photon. Rev.* **20**, 8608 (2021).